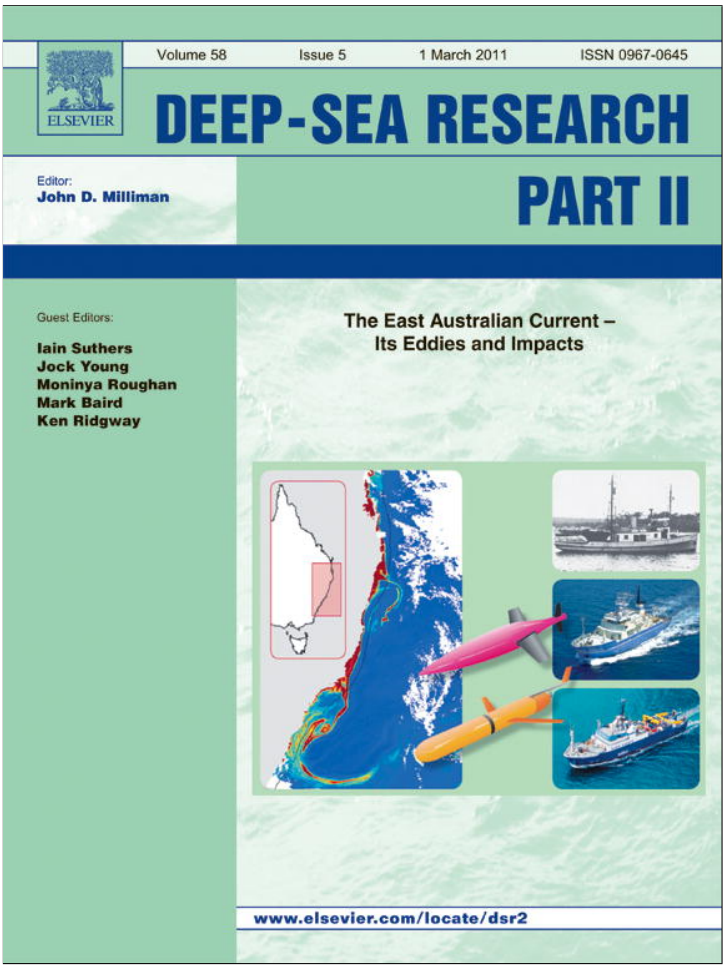

Deep-Sea Research II 58 (2011) 559–573

Contents lists available at ScienceDirect

Deep-Sea Research II

journal homepage: www.elsevier.com/locate/dsr2

Observed and simulated Lagrangian and eddy characteristics of the East Australian Current and the Tasman Sea

Gary B. Brassington [a,*], Nicholas Summons [b], Rick Lumpkin [c]

[a] Centre for Australian Weather and Climate Research, Bureau of Meteorology, PO Box 1289K, Melbourne, Australia
[b] University of Melbourne, Australia
[c] AOML, National Oceanographic and Atmospheric Administration, Miami, Florida, USA

ARTICLE INFO

Article history:
Received 2 October 2010
Accepted 2 October 2010
Available online 30 October 2010

Keywords:
Lagrangian drifting buoys
Western boundary currents
Mesoscale eddies
The Tasman Sea
The East Australian Current

ABSTRACT

New insights into the Lagrangian and eddy dynamical processes within the East Australian Current (EAC) and the Tasman Sea are presented. We briefly discuss the past campaigns undertaken to observe the EAC and the Tasman Sea eddies as well as the motivation to renew the deployment of drifting buoys into the EAC and the Tasman Sea. The specific features discussed are motivated by the recent observing campaigns using drifting buoys and the availability of high spatial- and temporal-resolution estimates of the ocean state and circulation from eddy resolving models. The interpretation of these features is also aided by other components of the ocean observing system. The dynamics presented includes: (a) transient EAC separation through a vortex dipole, (b) stratified vortex mergers and secondary circulation of EAC eddies, (c) eddy networks in the Tasman Sea and (d) formation and propagation of the EAC separation point. The importance of these dynamical features to the EAC and the Tasman Sea and their implications for the observing system and modelling are discussed.

1. Introduction

1.1. Variability of the circulation in the western Tasman Sea

Godfrey et al. (1980) make the following observation of the overall picture emerging from the observations, at that time, of the East Australian Current, "In contrast (to other western boundary currents), the flow patterns in the East Australian Current are so complex and variable that it is often difficult even to decide whether a single continuous current exists". The EAC is prominent amongst western boundary currents for the dominance of eddy kinetic energy (Stammer, 1997). Seasonal variability therefore accounts for a comparatively smaller fraction of the total variance in this region. An understanding of the instabilities and transient dynamical processes taking place is therefore necessary for a complete understanding of the EAC.

It has been established that the EAC has a distinct seasonal cycle (Ridgway and Godfrey, 1997). The EAC is characterised by relatively warm/fresh-water masses emanating from the Coral Sea. During the Austral summer the warm-water masses are sourced from the South Equatorial Current (Church, 1987), forming an observable shelf current along the shelf break of the Great Barrier Reef. During the Austral winter the coherent portion of the EAC weakens and retreats to a narrower region from southern Queensland to northern New South Wales. This is similarly confirmed by Schiller et al. (2008), which show the ratio of eddy kinetic energy to total kinetic energy for January and July (see Figure 7 of that article) in the Australian region based on the BLUElink ocean reanalysis (described in more detail in Section 2).

Historical observations of XBT's (Nilsson and Cresswell, 1981) and drifting buoys (Cresswell and Golding, 1979), discussed in more detail in the next section, have demonstrated the EAC is frequently composed of eddies that obscure the interpretation of the EAC as a boundary current. Ridgway and Dunn (2003) developed a high-resolution climatology for the Australian region from historical in situ observations. The average maximum alongshore transport of the EAC shows a local minima between 27 and 29°S. The local minimum lies to the north of the classical separation point between 30 and 34°S (Godfrey et al., 1980) and indicates a secondary EAC separation point. This is also associated with a local extremum in the mean dynamic topography indicating a recirculation (Ridgway and Dunn, 2003).

1.2. A short history of the Tasman Sea mesoscale experiments in the 1970s

Australian marine science has established a record for observing the ocean through innovative technologies and a golden period of observing the EAC and the Tasman Sea took place in the 1970s and 1980s. A collaboration between the Royal

* Corresponding author. Tel.: +61 3 9669 4170; fax: +61 3 9669 4660.
E-mail address: g.brassington@bom.gov.au (G.B. Brassington).

0967-0645/$ - see front matter © 2010 Elsevier Ltd. All rights reserved.
doi:10.1016/j.dsr2.2010.10.001

Australian Navy and the CSIRO undertook world leading studies of anticyclonic eddies defining many of the properties of this now classical type of eddy that is generated from the EAC flow separation. Early studies involved largely ship based hydrographic sections (Andrews and Scully-Power, 1976; Nilsson et al., 1977; Nilsson and Cresswell, 1981). In these early days eddies were individually named in an analogous way to atmospheric cyclone, for example Maria, Mario and Leo. A tradition that did not persist with the realisation of the complexity of eddy interactions (Airey, 1983) and the introduction of altimetry showing the abundance of eddies. Nonetheless, the EAC does generate only a handful of large-scale eddies each year, which have a dominant and persistent influence over the Tasman Sea circulation and perhaps there is a basis for reintroducing this practice amongst ocean forecasters.

Critical to early observational campaigns of the mesoscale were the use of drogued buoys. In 1972 a 3 m long transponder designed to be balloon-borne for high-altitude studies was put into a drifter and tracked by the French satellite EOLE. The drifter worked for 2 months and revealed meanders of the EAC. The drifter was a PVC/fiberglass spar buoy 5 m long. In 1977, drifters were used to track anticyclonic eddies in the EAC by the Nimbus satellite. These included eddies A–C, with B being studied for an year (Cresswell and Golding, 1979; Nilsson and Cresswell, 1981). In 1978 eddy J was studied for over a year with drifters and ship based hydrographic surveys (Cresswell, 1980 and others in a special issue of the Australian Journal of Marine and Freshwater Research). This early work was at the leading edge of demonstrating the instabilities of the EAC and the dominance of geostrophic turbulence in the Tasman Sea. The complexity of eddy–eddy interactions in the Tasman Sea was also observed during this period with the identification of a stratified merger of a new and an old anticyclonic eddy. In 1980/81 drifting buoys were used to track and study eddies Leo and Maria—and subsequently Mario after these two eddies coalesced (Cresswell, 1982; Cresswell and Legeckis, 1986). The coalescence was captured by the drifters and two ship surveys. The resulting eddy, Mario, was perhaps unusual in that it moved northward from a southern NSW location. CLS Argos was used for drifter tracking from this time onwards.

The deployment of drifting buoys in the Tasman Sea declined in the 1990s just as the satellite remote sensing and Argo profilers were emerging. Buoy deployments in the Indian and Southern Ocean over this period were supported by the Bureau of Meteorology to support meteorological forecasting. Operational buoy deployments sample the sea-surface temperature and sea-level pressure. Deployments are designed to sample the prevailing frontal systems. A similar operational schedule of buoys was deployed by the New Zealand meteorological service in the southern Tasman Sea for similar meteorological motivations.

1.3. A renewal of drifting buoy observations of the EAC

The introduction of remote sensing of the sea-surface temperature and altimetry provided the first images of the global ocean variability and demonstrated the dominance of eddy kinetic energy over much of the ocean. Over the past decade estimates for the mean dynamic topography, the global tides and other atmospheric corrections have provided sea-surface height anomalies from altimetry with an estimated precision of 5 cm (Laing and Challenor, 1999). The range of surface height anomalies for mesoscale eddies in the Tasman Sea is <1 m. Therefore eddies with surface height anomalies between 20 cm and 1 m are observable with variability larger than the expected error. The use of narrow-swath altimeters with repeat track periods of 10 days (Topex-Poseidon, Jason and Jason2) and 35 days (ERS1, ERS2 and Envisat) provides low temporal sampling which limits the wavelength of eddies that can be observed to greater than $\sim$150 km (Ducet et al., 2000). In the Tasman Sea this represents the large, deep and stable vortices that persist and dominate the local circulation. Features such as fronts and the secondary circulation of eddies are poorly observed from the available narrow-swath altimeters. A wide-swath altimeter (Fu et al., 2009) or constellations of narrow swath altimeters are required to adequately observe these features.

Drifting buoys approximately propagate with the ocean circulation thereby tracing a Lagrangian trajectory. Lagrangian trajectories can provide estimates of the mean velocity over different averaging periods from the mesoscale through climate scales. The precision of the estimates of surface circulation obtained is independent of the surface topography and is therefore complementary to altimetry observations (Hernandez et al., 1995). During the past decade the objectives of drifting buoys have targeted the mean upper-ocean circulation with a global distribution of 1250 buoys (Niiler, 2001), which represents an approximate density of one buoy for every $5^\circ \times 5^\circ$ surface area. This target density is adequate to capture mean circulation such as the Pacific Ocean tropical current system. In the Tasman Sea throughout the 1990s and the 2000s the drifting buoy deployments contributing to the global array declined and were shown to be below this target density (Summons et al., 2006). It was determined from a Lagrangian analysis of the BLUElink ocean Reanalysis (Schiller et al., 2008) that observing the EAC would require a targeted sampling strategy. A series of pilot experiments through a collaboration between the Bureau of Meteorology and the NOAA was initiated in 2007 (Brassington et al., 2007b) and designed to test a sustainable deployment strategy for the East Australian Current using volunteer ships.

A renewal of drifting buoy deployments has several motivations. The standard buoy design for the Surface Velocity Program (SVP; Lumpkin and Pazos, 2007) and analysis tools are now mature. Drifting buoys offer a reliable and high-yield observing system in terms of cost per observation and are suitable for sustained deployments. The drifting buoys provide a high quality in situ measurement of ocean currents and are a useful calibration/validation for the quality of other platforms such as the analysis of altimetry and HF radars. In addition, Lagrangian trajectories observe the total current and therefore provide in situ measurements of the mesoscale ocean circulation such as eddies, fronts and instabilities of boundary currents. In places where the circulation is closed, such as eddies, drifting buoys can undergo multiple orbits to provide sufficient observations to interpret their dynamics (Richardson et al., 2000, Font et al., 2004, Sangra et al., 2005, Brassington, 2010).

In places where the circulation is not closed, where the buoys will have a relatively short residence time, a higher density or repeated sampling is required to provide sufficient observations to interpret the dynamics. Many oceanic processes such as heat and momentum transport, and biological processes of larval dispersal, are controlled by Lagrangian processes. Lagrangian observations provide essential observations for evaluation of these models (e.g., Chiswell, 2009; Chiswell and Rickard, 2008). Further, Lagrangian observations are also critical to evaluation of models for use in Search and Rescue (Davidson et al., 2009) and Marine Accident and Emergency Service (Hackett et al., 2009) applications. The standard buoy also includes a temperature sensor that provides a bulk measurement of sea surface temperature with a known error characteristic. The temperature observations are routinely used for calibration/validation of satellite SST products that improve the detection of biases and time-dependent errors (Donlon et al., 2002, 2009).

This paper organises results from recent observational experiments and model/observation assimilated analyses, focusing particularly upon the mesoscale variability and processes that are a permanent feature of this region. The observations discussed and the model simulations used are presented, and the specific methods that have been developed and recent techniques in pattern matching have been adapted to aid in interpreting the observations and model simulations are described.

2. Methods

2.1. Observations

A multi-year drifting buoy experiment was designed to determine if the volunteer observing ship (VOS) program could be used as a cost-effective method for seeding the EAC and the Tasman Sea (Brassington et al., 2007b, 2008). It is difficult to sustain observations in a boundary current with surface drifting buoys due to the relatively short period that the buoys are resident within the current and a regular deployment strategy was explored. The experiment made use of two Australian Volunteer Observing Fleet ships, the Capitaine Tasman and the Forum Samoa II, that occupy the PX30 XBT line between Fiji and Brisbane approximately every two weeks (see Fig. 1). This XBT line transects the EAC at ~27°S where the EAC is a semi-permanent coastal current. The drifting buoy experiment was designed to deploy NOAA buoy pairs (separation of 5 km) from the VOS ships where they traverse the EAC. The streamlines of the mean surface circulation are shown as contours in Fig. 1. These contours show that the PX30 line crosses the EAC where it exhibits the strongest mean flow. The two-week cycle of the VOS ships provides repeat deployments to observe the temporal variability of the Lagrangian behaviour of the EAC. The precise position to deploy the buoys was designed to (a) observe the EAC, (b) avoid potential loss of buoys through coastal groundings and (c) achieve long (maximum) deployment periods. The location was selected through the use of the BLUElink ocean reanalysis (BRAN) (Oke et al., 2008; Schiller et al., 2008). Lagrangian trajectories were traced using the BRAN surface currents with corrections applied for current shear and surface winds (Niiler et al., 1995). An example of the synthetic trajectories is shown in Fig. 2 for a launch date of 7 March 2002. The deployment location was determined by objectively assessing the probability of each location for a range of start dates against the above mentioned design criterion. The observed deployment positions for the experiments are shown in Fig. 1 as white circles.

The buoy experiment has been deployed for each year since 2007 to assess the reliability of these deployments for different deployment times and interannual variability of the EAC. The buoys used in the EAC experiments consist of a surface buoy tethered to a holey sock design drogue positioned at 15 ± 7.5 m. This drifting buoy is designed to follow the surface currents of the ocean and its behaviour has been extensively observed and calibrated (Niiler et al., 1995). The buoys transmit their position and surface observations to satellites ~20 times per day, providing an estimate of the trajectory from which many properties can be derived. The observations from these experiments capture several events that highlight some of the mesoscale behaviour of the EAC. Quality controlled position and SST observations are obtained from NOAA.

Estimates of daily average sea-surface temperature (SST) are obtained from OSTIA (Stark et al., 2007) and from a daily composite image of SST observations from MTSAT-1R. OSTIA is an operational high-resolution SST daily analysis of the foundation temperature (refer to the online definitions maintained by the Global High Resolution Sea Surface Temperature (GHRSTT) science team, http://www.ghrsst.org/SST-Definitions.html). Foundation temperature specifically refers to the near-surface temperature of the ocean excluding diurnal skin effects and is most relevant to the ocean state and dynamics. In practice, observations are withheld from the analysis as being impacted by diurnal skin effects based on the time of day and the magnitude of the 10 m winds as a proxy for near-surface mixing (Donlon et al., 2002). MTSAT is a geostationary satellite operating at a longitude of 135°E and provides one full scan of skin SST each hour. The processing of MTSAT retrievals has been problematic with an

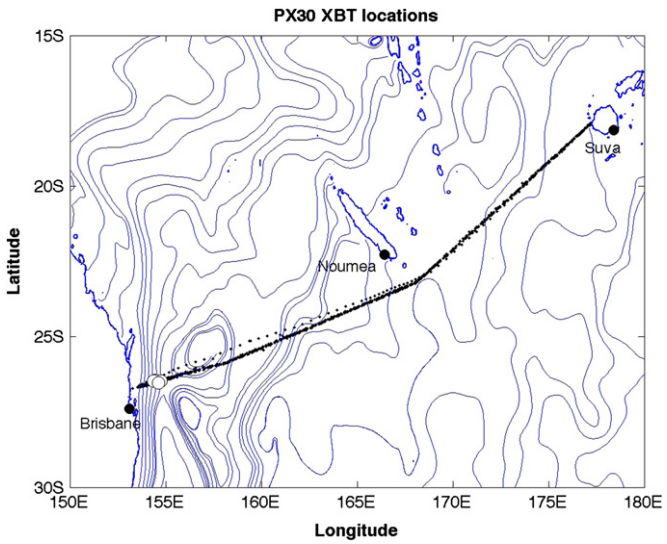

Fig. 1. Position of each XBT deployments along the high-density PX30 line for the period (5 February 1993–12 October 1998). Contours show the streamlines from the mean surface circulation from BRAN. The PX30 line transects near the coast where the EAC is a semi-permanent current. The initial positions of the drifting buoy deployments for 2007 and 2008 are shown as white circles.

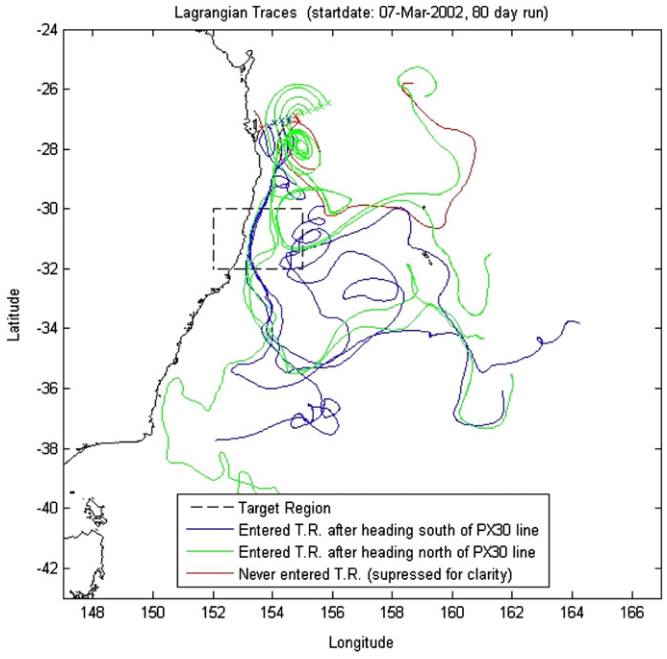

Fig. 2. Lagrangian trajectories with origins along the PX30 line near the Australian east coast and start time of 7 March 2002 from the BLUElink ocean reanalysis version 1. The Lagrangian trajectories were assessed for the probability of observing the target region, coastal grounding and long-period deployments.

algorithm developed jointly between the Bureau of Meteorology and the NOAA, which includes bias corrections and cloud clearing algorithms. Each scan individually provides information between clouds which limits the coverage per scan during the period of interest; however, through the advection of clouds the coverage of multiple scans is sufficient to provide an estimate of the skin SST at near complete coverage. The MTSAT SST estimates for the Tasman Sea are obtained by compositing the 24 scans into a single image using the median of the available valid values for each pixel. This method produces an image that is relatively noisy compared with a conventional optimal interpolation (OI) approach. However, the gain is that it is able to preserve fine scale features compared with analyses products such as OSTIA.

2.2. Model products

High spatial- ($0.1^\circ \times 0.1^\circ$) and temporal- (daily mean) resolution estimates of the ocean state and circulation of the Tasman Sea are obtained from systems developed by the BLUElink project, a collaboration of the Bureau of Meteorology, CSIRO and the Wealth from Ocean Flagship and the Royal Australian Navy. Both the BLUElink ocean ReAnalysis (BRAN; Schiller et al., 2008) and the operational BLUElink Ocean Model, Analysis and Prediction System (OceanMAPS; Brassington et al., 2007a) share a common ocean model and data assimilation software but use different observations and surface flux products (Seaman et al., 1995). An important distinction also lies in the implementation of the data assimilation system in OceanMAPS and BRAN. For example, the number of ensemble members used to form the background error covariance in OceanMAPS (72) is less than in BRAN (144) due to computational constraints and the frequency with which an analysis is applied 3/4 days (7 days). Other subtle differences reside in the revisions of the software due to the development cycle. BRAN is used to research and develop major revisions to the system components which once robust for the delayed mode are adopted into the offline research OceanMAPS and extensively trialled before implementation into operations. At the time a new revision is being implemented into operations a new revision to BRAN is being developed in parallel.

The common ocean model, Ocean Forecast Australia Model (OFAM; Schiller et al., 2008), is an implementation of the GFDL Modular Ocean Model version 4 (Griffies et al., 2003). Details of the specific implementation are described in Schiller et al. (2008). Relevant features are the implementation of a global grid with course resolution away from Australia and uniform ($0.1^\circ \times 0.1^\circ$) resolution in the Australian region (90–180°E, 75°S–16°N). At each high-resolution boundary the resolution is smoothly graduated to minimise the generation of noise through wave reflection. The vertical resolution is a uniform resolution of 10 m over the top 200 m and smoothly graduated to a resolution of 550 m and a total depth of 5500 m.

The data assimilation system common to OceanMAPS and BRAN, the BLUElink Ocean Data Assimilation System (BODAS; Oke et al., 2008), is a mulit-variate, ensemble, optimal interpolation scheme. That is it resolves the least squares optimal interpolation analysis equation in observation space; however, the background error covariance is estimated by a stationary ensemble of model state anomalies. Each state anomaly is constructed by removing the seasonal mean from a 3-day average of a multi-year spinup integration forced by ERA40. This error model assumes that the background errors can be of the scale and have covariance relationships of the order of the mesoscale signal.

2.3. Lagrangian trajectory analysis

Lagrangian tracks from within an eddy have a high likelihood of orbiting the central anomaly and propagating with the eddy for a period of time. The simplest information that can be obtained about the eddy from these trajectories is the orbital speed and the position of the eddy's mean position (and therefore its mean speed).

Brassington (2010) has demonstrated that in addition to this information, a single Lagrangian track can provide information on the anisotropy of the eddy, secondary rotation and horizontal divergence. The extended analysis is based on the assumption that the points on a material surface within an eddy evolve smoothly in time. Using spline interpolation in time and coordinate transformations an instantaneous representation of the material surface can be obtained. The estimated material surface from an ocean eddy to close approximation can be fitted to an ellipse to provide characteristics of area, orientation and eccentricity.

As an example consider the drifting buoy trajectory from WMO55916 and WMO55924, which orbit an eddy within the EAC

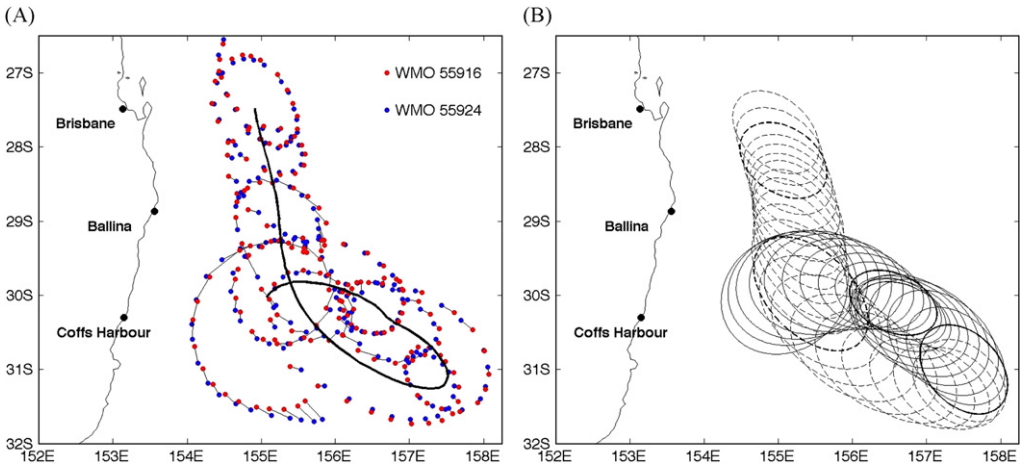

Fig. 3. (A) The positions and separation of a buoy pair, WMO55916 and WMO55924, whilst orbiting an anticyclonic eddy separating from and regressing back toward the EAC. Overlayed is the ellipse centroid or mean trajectory of WMO55916 (Brassington, 2009). (B) The daily estimates of the surface material boundary fitted to an ellipse observed by the drifting buoy WMO55924 between 1 March and 11 April 2007. Every 10th day since the buoy was deployed from 21 February is shown in bold. The ellipses in the southeastward trajectory are shown as dotted lines for clarity.

shown in Fig. 3A. The corresponding set of instantaneous material surface ellipses derived from this method is shown in Fig. 3B. The centroid from these ellipses provides a least squares estimate of the mean trajectory shown in Fig. 3A. The ellipses show a continuous change in area with a distinct surface convergence visible during the regression westward, indicating a downwelling in the central core of the eddy.

2.4. Eddy tracking techniques

An eddy tracking method based closely on Clifford convolution is applied to velocity fields from BRAN. The Clifford convolution has been employed previously by Ebling and Scheuermann (2005, 2003) and Heiberg (2001), and was shown to provide a robust, noise-tolerant method for identifying flow features for a range of applications from the field of fluid mechanics. The general form of the Clifford convolution in two dimensions can be defined as the integral over the domain D of the inner product of a template vector field M with that of the normalised flow field U to identify points of maximum correlation:

$$z(r) = \iint_D \langle M(\xi), U(r+\xi) \rangle d\xi \quad (1)$$

where $\xi \in D$ and r represent a position vector in the target velocity field U. Local extrema represent the centroid of maximum correlation. This method is repeatedly applied to the velocity field to identify specific properties of the eddies in the model field. A template for body rotation (see Fig. 4A) is used to identify the centres of rotating fluid motion. The template is defined for a unit circle with $u_\theta = r$ for all $r < 1$ and $u_r = 0$ in polar coordinates (or equivalently in Cartesian coordinates, $u = y$, $v = -x$ with a mask set true for $r < 1$).

Eddies in general are anisotropic with a specific orientation. This orientation is found using a simple template with a saddle point flow field (see Fig. 4B), which is rotated about an origin of each vortex centre to find maximum correlation. The template is defined by $u_r = r \cos 2\theta$ and $u_\theta = r \sin 2\theta$ in polar coordinates (or equivalently in Cartesian coordinates, $u = x$, $v = -y$ with a mask set true for $r < 1$). This method has similarities to Okubo–Weiss (Okubo, 1970; Weiss, 1991) but adopts a topological approach for identifying the effects of strain and shear on the flow. The flow field of an eddy is assumed to be, to a close approximation, a superposition of flow elements that can be robustly determined by the extremum in the Clifford convolution. The pattern search approach applied to a vortex can be extended to cross-correlate with the element of an elliptical flow pattern to define the eccentricity and area of the coherent elliptical flow to track the time rate of change of these properties.

A *priori* we assume that the velocity field of the Tasman Sea is dominated by two-dimensional turbulence and therefore to within a small perturbation vortices are axially aligned with the gravitational vector (Pasquero et al., 2007; Beron-Vera et al., 2003). Three-dimensional eddy tracking is derived through a two-step process. In the first step, the cross-correlations are applied to each layer of the velocity field. The position of all vortices within the velocity field can be identified as local maxima. The vertical extent of the vortices is then identified by searching for a local maximum in the adjacent layer within a small perturbation of the vertical axis.

3. Results and discussion

3.1. Transient EAC separation through a vortex dipole

A pair of drifting buoys was deployed on 21 February 2007 into the surface circulation of an anticyclonic eddy within the EAC (Brassington et al., 2007b; Brassington, 2010). If we assume the analysed sea level anomaly (not shown) is in geostrophic balance the geostrophic speed is estimated to be $-0.53\ \mathrm{m\ s^{-1}}$, which compares well to the observed tangential speed of the two buoys of 0.61 and $0.64\ \mathrm{m\ s^{-1}}$, respectively. The difference is partly accounted for by the mean eddy propagation speed estimated to be $<0.17\ \mathrm{m\ s^{-1}}$ at the time of deployment. The buoys remained within the surface circulation of the eddy for more than 60 days completing 9 orbits as a close pair (see Fig. 3). The mean trajectory of the drifting buoys (see Fig. 3A) shows that the eddy propagated southward within the EAC, approximately following the potential vorticity contour (not shown) for the first 20 days. Between 29 and 30°S the mean trajectory shows the eddy separates from the coast before accelerating south-eastward. Simulated sea-level anomalies from BRAN indicate that a cyclonic circulation had formed over the continental slope at 28–29°S (see Fig. 5A), which corresponds to a region that has been previously identified for topographically induced upwelling (Oke and Middleton, 2000). The simulation shows that as the anticyclonic eddy propagates south it interacts with the cyclonic vortex and moves southward while intensifying its gradient in sea-surface height (Fig. 5A–G).

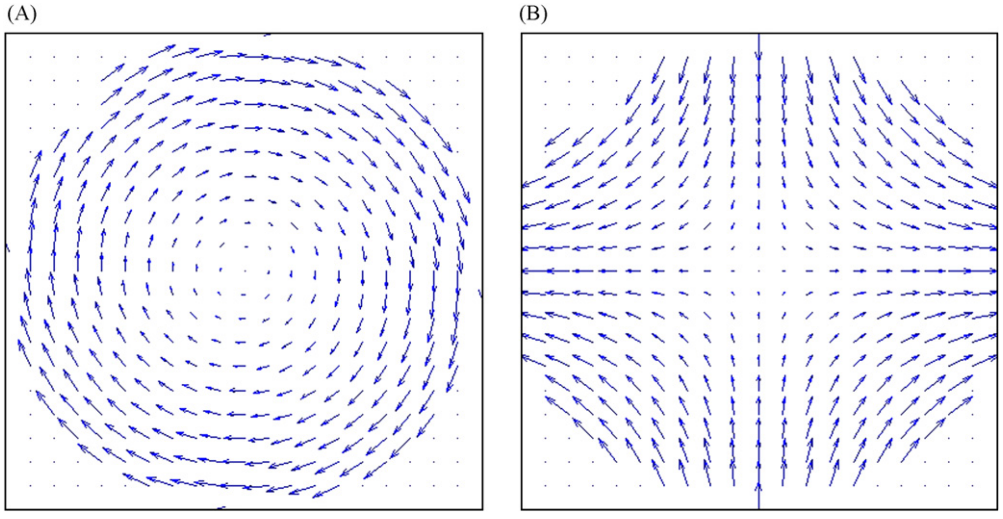

Fig. 4. Pattern matching templates M defined for the domain $x \in [-1\ 1]$ and $y \in [-1\ 1]$: (A) $u = x$, $v = -y$ and rotating flow and (B) $u = y$, $v = -x$ and saddle point flow. Each template has had a mask applied where mask = 1 for all $r \leq 1$.

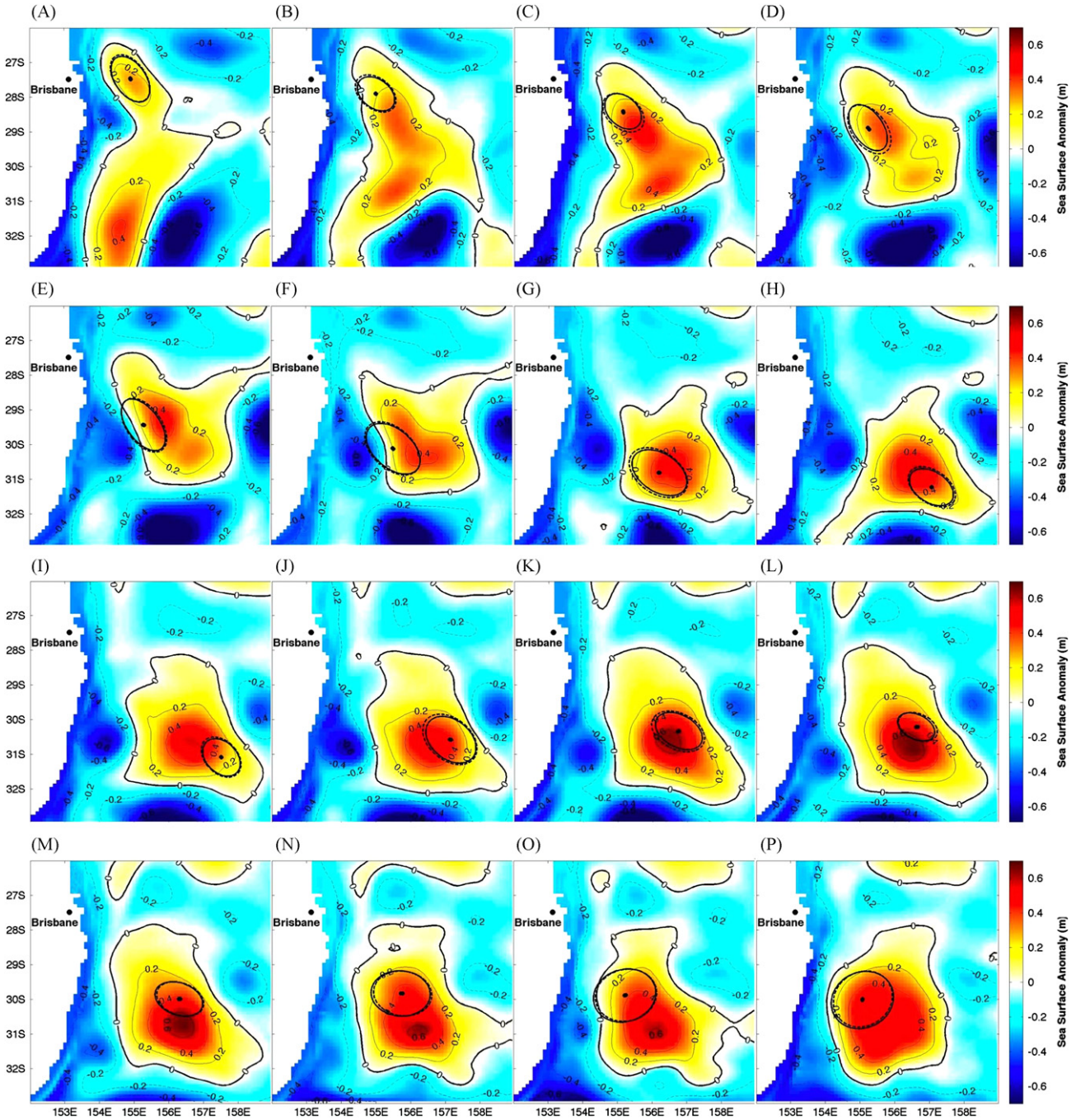

Fig. 5. Daily averaged reanalysed sea level anomaly over the Tasman Sea from BRANv2.2 (Oke et al., 2008): (A) 27 February, (B) 2 March, (C) 5 March, (D) 8 March, (E) 11 March, (F) 14 March, (G) 17 March, (H) 20 March, (I) 23 March, (J) 26 March, (K) 29 March, (L) 1 April, (M) 4 April, (N) 7 April, (O) 10 April and (P) 12 April 2007. Overlayed are the estimated surface ellipse corresponding to each day.

The formation and intensification of a coastal cyclonic vortex is also visible in the daily composite SST observations from MT–SAT, shown in Fig. 6. The leading edge of the cyclonic vortex is traced by a small plume of cooler coastal water that circulates from the coast by the offshore flow between the vortex dipole (Fig. 6A) and returns around the eddy (Fig. 6B). The ocean analysis in Fig. 5 shows that the coastal cyclonic vortex and EAC anticyclonic vortex propagated for a short period as a vortex dipole displacing the anticyclonic eddy southeast away from the coast. This event formed a transient separation of the EAC that persisted for approximately 1 month. The consistency between the analysed simulation (Fig. 5A–F) and observations (Figs. 3A and 6) indicates that the dipole separation at this location is not sensitive to the errors in the model representation of the cyclonic and anticyclonic eddies.

The separation point is equatorward of the classical separation position ~32°S (Godfrey et al., 1980). The buoy observations demonstrate an additional transient mechanism for EAC separation that was not been previously identified. Transient flow separation on the coastal and the Tasman Sea circulation can lead to important impacts per event. For example the anticyclonic eddy that separated persisted for several months providing anomalous heat content off the northern NSW coast during the Austral winter. The eddy was located just to the south of

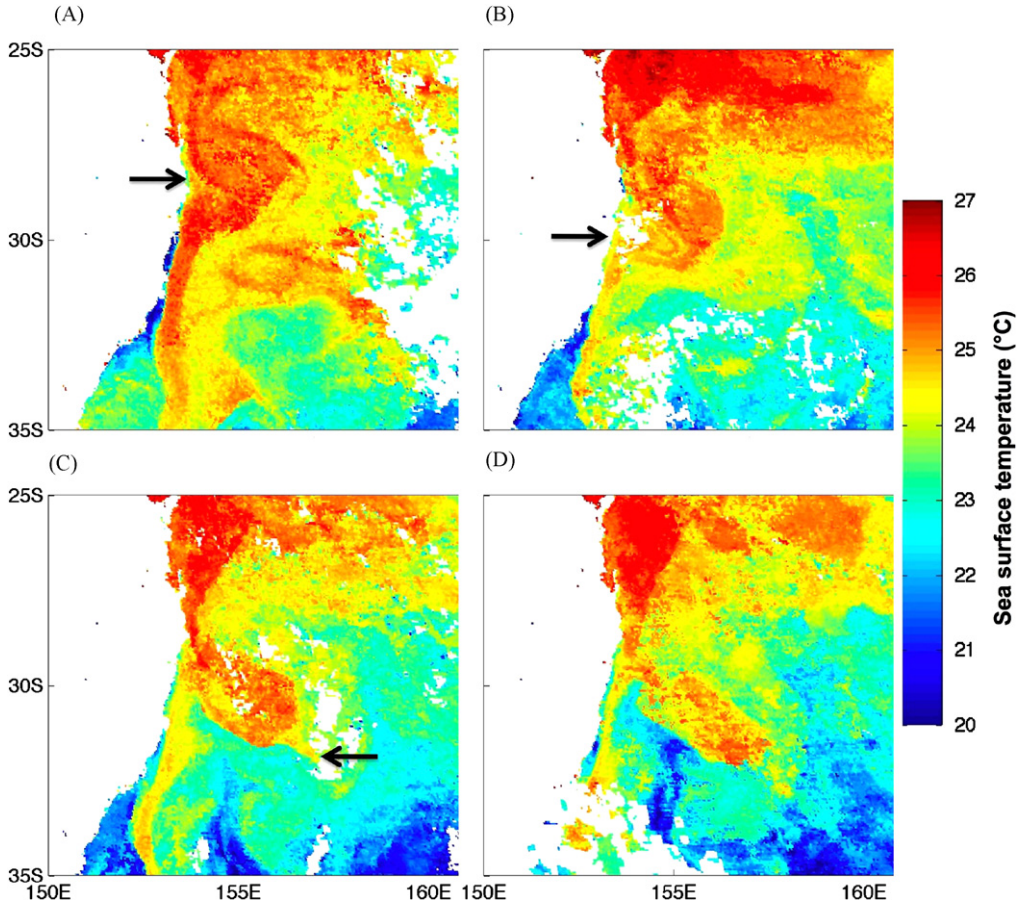

Fig. 6. Daily composite sea surface temperature from the geostationary satellite MTSAT: (A) 2 March, (B), (C) 14 March and (D) 16 March 2009. The arrow locates a narrow trace of cooler sea-surface temperatures.

Newcastle when an east coast cut-off low (McInnes et al., 1992) intensified and became famous for the Pasha Bulka cargo ship that was washed ashore. The same event also resulted in fatalities in Newcastle from flash flooding. Similarly the intensification and propagation of the cyclonic vortex has important impacts for biological productivity on the shelf (Tranter et al., 1986; Oke and Middleton, 2001).

Statistically, the importance of the transient flow separation is determined by the frequency and period of such events. In addition to previous coastal observing campaigns (e.g., Oke and Middleton, 2000; Roughan and Middleton, 2002), the transient formation of a shelf cyclonic circulation was observed by drifting buoys in the 2008 EAC experiment (Brassington et al., 2008). The Lagrangian trajectories of the six buoys deployed during that experiment are discussed later in Section 3.4 (see Fig. 10). The third pair of buoys shows a coastal disturbance of the EAC forming within the period of two weeks (the period between deployments) at approximately the same location.

A survey of the historical evidence prior to 1980 (Godfrey et al., 1980) pointed to an EAC separation likely between 30 and 34°S with a specific southern limit point identified as Sugarloaf point, (32.16°S) from which the EAC no longer continued as a boundary current. This apparent limit point in the observations and associated circulation of the Tasman Front has been the focus of several studies. Theories have focused on Sverdrup dynamics and the role of New Zealand in blocking mass flux based on the island rule, local winds, local shelf topography, abyssal topographic control and nonlinear dynamics (Godfrey, 1989; Marchesiello and Middleton, 2000; Tilburg et al., 2001; Ridgway and Dunn, 2003; Wilkin and Zhang 2007).

Ridgway and Dunn (2003) developed a high-resolution climatology for the Australian region from historical in situ observations. The average maximum alongshore transport of the EAC shows a global minimum at the above mentioned classical separation point. However there is also shown a local minimum in alongshore transport between 27 and 29°S. The local minimum lies equatorward of the classical separation point and has been interpreted to be an indication of a secondary EAC separation (Ridgway and Dunn, 2003). The observed transient EAC separation observed in 2007 (and 2008 discussed in Section 3.4) offers a plausible mechanism to explain the local minima in the mean alongshore transport identified by Ridgway and Dunn, (2003).

3.2. *Stratified vortex mergers and secondary circulation of EAC eddies*

An important feature of the ocean simulation shown in Fig. 5 for the separation of the EAC anticyclonic vortex (now EAC eddy) is the northward propagation of another Tasman Sea anticyclonic eddy (now Tasman Sea eddy) originating to the south at 31°S. The Tasman Sea eddy propagates north-eastward ahead of the EAC eddy in Fig. 5A–F and subsequently merges with the EAC eddy in the simulation. Noting that the drifting buoys show that the surface of the EAC vortex remained stable throughout the event indicates that the eddy merger did not lead to a shear typical of

two-dimensional turbulence. Recent literature on geostrophic vortex mergers has identified several types of mergers depending on the relative stratification and rotation of the original eddies (e.g., Reinaud and Dritschel, 2002; Bambrey, 2007). Unstratified mergers of similar magnitude vortices lead to the classical shearing of the vortices and a major disruption to the surface circulation. Stratified vortex mergers in contrast can occur with negligible shear to the surface circulation and in extreme cases can coalesce with minimal disruption to either vortexes.

The drifting buoys shown in Fig. 3A continue to orbit a coherent surface circulation with minimal disruption during the period of the vortex merger. The time rate of change of the ellipse properties shown in Fig. 3B of centroid, area, orientation and aspect ratio shows a continuous change throughout the first 60 days including the vortex merger. Although the method used (Brassington, 2010) is based on interpolation, a continuum is unlikely to occur for a large shear vortex merger. The 24 h average sea-surface temperature analyses shown in Fig. 7 also demonstrate that the SST remains anomalously warm after the merger with the maximum temperature lying within the ellipse. The majority of impact occurs after the initial merger in the form of secondary circulation adjustment as observed by the convergence of the ellipse area in Fig. 3B between the 30th and 40th day from the initial deployment.

During the same period an Argo float surfaced in the region on 26 February, 8, 17, 27 March, and 6 April 2009 as shown in Fig. 7. Using the estimated ellipse centroid as a reference, the Argo in situ profiles of temperature and salinity relative to the distance from the centroid are shown in Fig. 8. The profiles within the ellipse demonstrate that the interior exhibits the temperature/salinity anomalies consistent with an anticyclonic eddy extending over the top 700 m. The first three surfacing positions shown in Fig. 6A, C and F occur prior to the arrival of the separated eddy. The surfacing positions indicate there was weak flow throughout

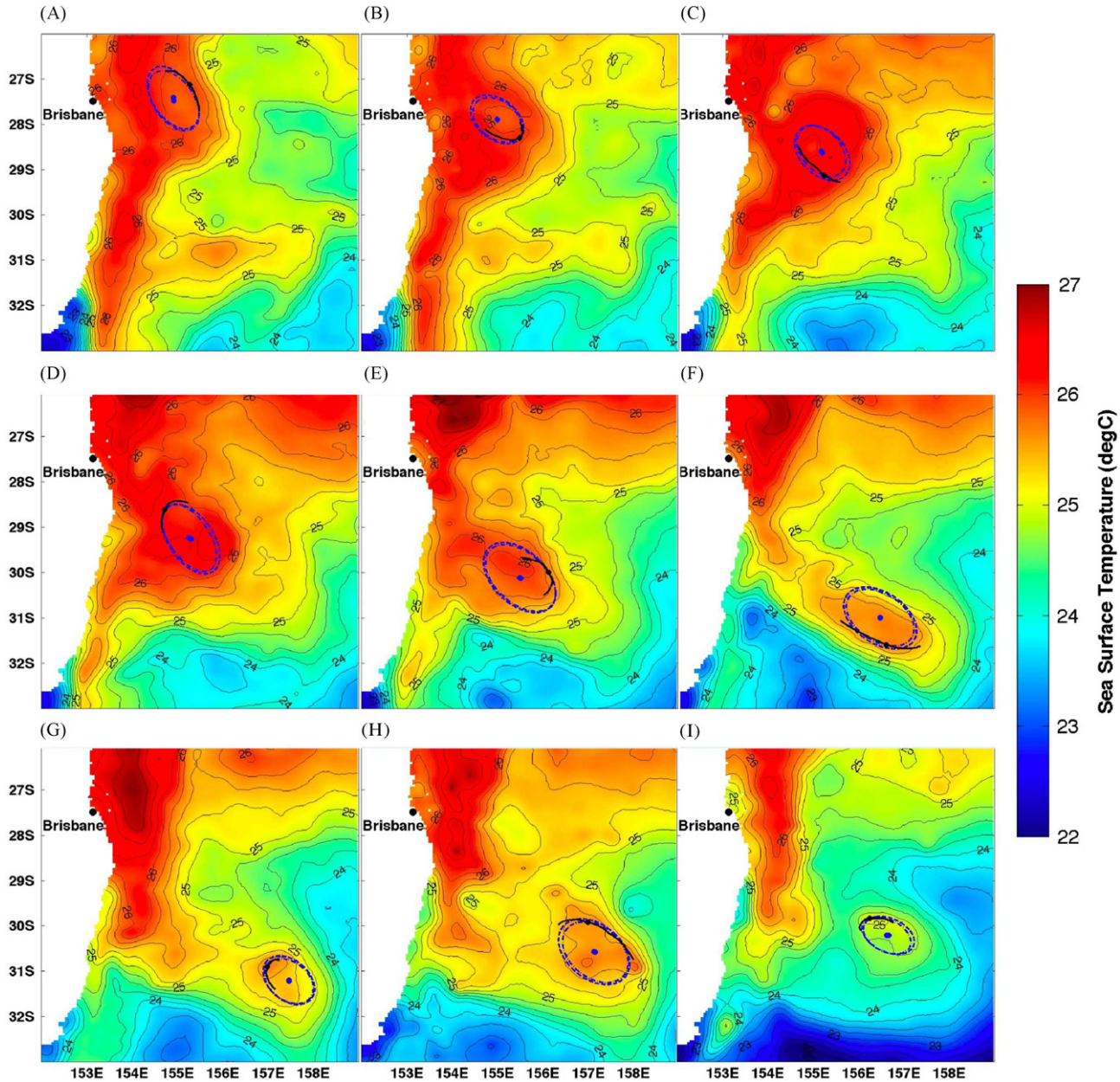

Fig. 7. The SST of the Tasman Sea for (a) 26 February, (b) 2 March, (c) 8 March, (d) 10 March, (e) 14 March, (f) 18 March, (g) 27 March (h) 1 April and (i) 6 April 2007. Overlayed are the buoy trajectory ± 0.5 day about each day and the estimated ellipse material surface. The surface position of Argo profiles is shown as a cross (x).

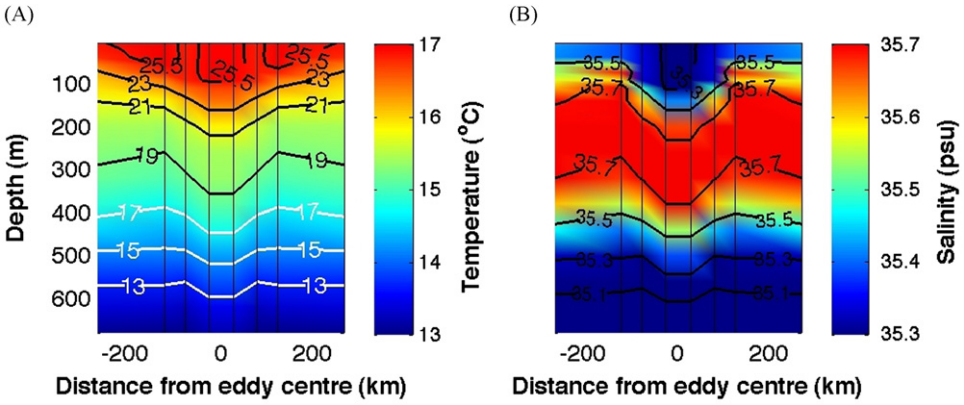

Fig. 8. Argo profile observations shown in Fig. 7: (A) temperature structure of the vortex estimated by the Argo profiles positioned relative to the distance from the vortex centroid estimated in Fig. 3B and (B) same as (A) but for salinity. The profiles shown as vertical black lines sorted by distance from the centroid correspond to: 27 March (Fig. 7G), 6 April (Fig. 7I), 18 March (Fig. 7F) and the background 8 March (Fig. 7C).

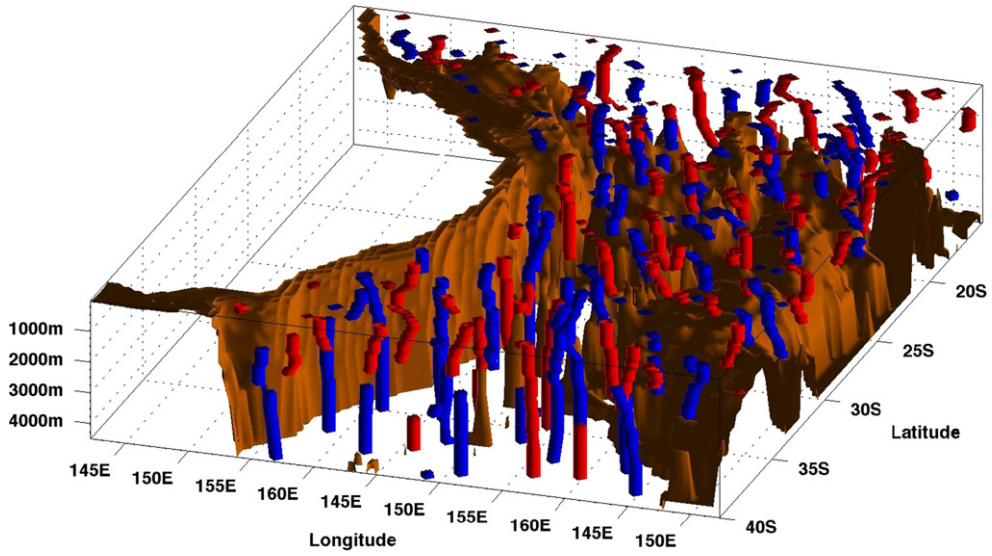

Fig. 9. Anticyclonic (red) and cyclonic (blue) vortices in the Tasman Sea identified by a pattern matching method and their coherent circulation in the vertical. The analysis was applied to a day average velocity field based on real-time analysis of OceanMAPS (Brassington et al., 2007a) for 4 April 2009. (For interpretation of the references to colour in this figure legend, the reader is referred to the web version of this article.)

the upper 2000 m. The profile on the 18th March coincides with the arrival of the leading edge of the separating vortex (Fig. 7F) and observes a shallow warm layer ~150 m and a cooler abyssal temperature compared to the background (Fig. 8A). This indicates that the northward propagating eddy from the model simulation shown in Fig. 5G is slightly ahead of the true ocean. The two profiles that observe within the interior of the surface circulation of the eddy occur after the eddy merger. Both profiles show temperature and salinity anomalies characteristic of an anticyclonic eddy extending to depths >500 m (Fig. 8A–B). During this period the surface locations show the Argo float has propagated in a consistent anticyclonic motion. Subsequent to the merger the vortex propagates westward and the surface layer becomes weakly divergent leading to the ejection of the drifting buoys.

Stratified vortex mergers in the Tasman Sea have been previously identified (Cresswell, 1980, 1982). Two vortices were observed using hydrographic surveys to identify a unique isothermal core of differing densities. A merged eddy was later surveyed and was found to be composed of isothermal layers that had originated in the first two eddies. It was noted in that study that the deeper vortex originated south of the merger location and propagated northwards. This propagation pathway has similarities to that identified by Wilkin and Zhang (2007) using EOF analyses of the SST and SLA observations. This pattern was labelled a wave-mode, however the features being discussed here are deep core eddies, not waves.

With the existence of stratified vortex mergers it is reasonable to ask how frequently might such events occur. We apply the pattern matching method to a single daily average velocity field from the behind real-time analysis of OceanMAPS (Brassington et al., 2007a) for the Tasman Sea on 4 April 2009 (see Fig. 9). The anticyclonic vortices are shown in red and cyclonic vortices in blue. Coherent vortices of both anticyclonic and cyclonic eddies (as simulated by the model) can extend to full depth (>4000 m) with a larger population of cyclonic vortices in the southern Tasman Sea. The surface layer has a higher concentration of vortices and eddy kinetic energy. These vortices are composed of full depth vortices and shallow vortices, which can be newly formed vortices, vortices that have sheared away from the deep vortex and other mechanisms. The vortices at abyssal depths are largely composed of full-column vortices or residual vortices from

a shearing event. Many of the full-depth vortices shown in Fig. 9 are non-axially aligned with the gravitational vector indicating they are under stress.

As indicated above there are examples of stratified vortex mergers in the Tasman Sea; however, the prevalence of deep vortices and their persistence has not yet been identified in observations. In the model simulation deep vortices exhibit a weak decay and persist for a period of several days, which is sufficient to undergo stratified vortex interactions with other surface vortices. The model simulations therefore suggest that stratified mergers could occur frequently. The reliance on poorly known statistical relationships to project the sea-level anomalies to adjust the temperature/salinity at depth as well as insufficient knowledge of the turbulent dissipation rates limit the quality of the abyssal ocean estimate. The properties and interactions of these deep vortices are nonetheless important for eddy-resolving models for their influence on the surface vortices.

3.3. Eddy networks in the Tasman Sea

A characteristic of the surface circulation of geostrophic turbulence is that eddies are quasi-stable acquiring rotational inertia that persists for a period of time propagating and interacting with the mean flow and other eddies. By contrast the circulation of geostrophic turbulence between stable eddies tends to be unorganised and chaotic (Beron-Vera et al., 2003). The historical record of surface drifting buoys demonstrates that buoys deployed within the surface circulation of eddies frequently remain for a period completing several orbits (Rupolo, 2007). An example of this is shown in Fig. 3. The surface layer of the eddy in this case remained stable whilst the surface vortex underwent significant interaction. The two buoys exhibit distinct periods of convergence and divergence in response to eddy interactions with the abyssal layer. Dispersion of drifting buoys out of an eddy in general coincides with a disturbance such as the decay phase of the eddy or through shearing induced through vortex interaction. Drifting buoys can also be entrained into the surface layer of eddies; however, this occurs at specific times and locations such as formation, decay and interaction that result in a disruption/shock to the rotational circulation. The probability for a buoy to be entrained into an eddy is low and the majority of drifting buoys propagate in the flow between vortices (Provenzale, 1999; Pasquero et al., 2007).

We explore this behaviour in the Tasman Sea applying the pattern matching algorithm, described in Section 2.3, for the template of solid body rotation, to four daily average surface velocity fields from BRAN. The four daily means are separated by a 7-day interval, beginning on 17 March, and shown in colour in Fig. 10. Vortices, either cyclonic or anticyclonic, can be identified as local extremum shown in red, which are above a given threshold. Many of the local extremum show extensions where the Clifford convolution (refer to Section 2.4) is of medium magnitude. These extensions are composed of shear flow that provides positive contributions where the shear flow aligns with the template and small negative contributions where the template is normal to the flow. These extensions provide a metric that qualitatively captures the non-local influence of coherent vortices described by Pasquero et al. (2007).

The BRAN velocity field, in Fig. 10, is characterised by a spectrum of eddies from the near grid scale $\sim$40–200 km. Larger eddies occur near the EAC separation point and along the coast while the southern Tasman Sea has many smaller vortices. In addition to identifying local maxima the pattern-matching algorithm identifies secondary properties of orientation, eccentricity and area. The time rate of change of these properties relate to the rotational momentum budget and divergence of the surface circulation of the eddy. We identify three eddies labelled A, B and C in Fig. 10 to track the evolution of these properties. Eddy A is that which was observed by the drifting buoy shown in Fig. 3. On 17 March (Fig. 10A) the surface motion is anisotropic and oriented in alignment with a shear flow emanating from the shelf. Eddy A subsequently becomes detached from the EAC and begins to enlarge the area of coherent flow and becomes more isotropic (Fig. 10B and C). Throughout this propagation eddy A is interacting with a cyclonic vortex to the south and north that remains aligned with a shear flow. Eddies B and C are eddies to the east of Bass Strait and Tasmania. Eddy B is isotropic on 17 March and shows an increase in shear and anisotropy before declining (Fig. 10D). Eddy C propagates eastward and both increase in size and become more isotropic. In general the circulation in the Tasman Sea is occupied by a small number of large, near isotropic eddies that have a long timescale. The remaining circulation is composed of a spectrum of smaller vortices that exhibits vigorous interaction and shorter timescales.

In addition to identifying the location of vortices, the Clifford convolution for the rotation template also shows a network of medium magnitude convolutions. In many instances these extensions link up between like-signed eddies, indicating the direction water masses are being exchanged. Many of the eddies show orientations and eccentricities that are in alignment with these lines. Two examples of these are indicated by the red arrows in Fig. 10C and D. In some instances this is the result of a shear flow that leads to the growth of vortices analogous to Capet et al. (2008) and in other instances it occurs through the transient linking between the eddies. Many examples occur where multiple eddies link up forming long networks providing extended circulation pathways and these pathways can persist. The flow speed or streamlines associated with these fronts are of the order of the rotational speed of the vortices and therefore is an efficient mechanism for the transport of water mass. This mechanism can transfer water masses over the distance of the chain of eddies, which can be up to several eddy wavelengths. An animation of this metric shows that eddy chains have a shorter timescale than the eddies themselves. The classical representation of eddy fluxes in climate models does not adequately represent this process and alternative parameterisations have been suggested (Pasquero et al., 2007).

The ocean circulation between eddies is observed by all drifting buoys not entrained within the closed circulation of eddies or directly deployed onto eddies. Since the probability of entrainment into eddies is low, the majority of drifting buoys observe this part of the circulation. This portion of ocean circulation has a lower steric-height anomaly comparable to the known error and therefore cannot be precisely observed by satellite altimetry. Therefore Lagrangian trajectories provide robust, frequent and complementary information on this part of the circulation. Techniques to assimilate Lagrangian information into Eulerian models have been developed (Molcard et al., 2007). The density of drifting buoy observations required to constrain the ocean circulation is flow dependent. Molcard et al. (2007) show the sensitivity of the analysis of a simple model to numbers of Lagrangian trajectories. The impact in the presence of altimetry is unknown and needs to be subjected to the same observing system design experimentation as other parts of GOOS (Oke et al., 2009).

3.4. EAC separation point reattachment

During the 2008 drifting buoy campaign (Brassington et al., 2008) three drifting buoy pairs were deployed along the PX30 line

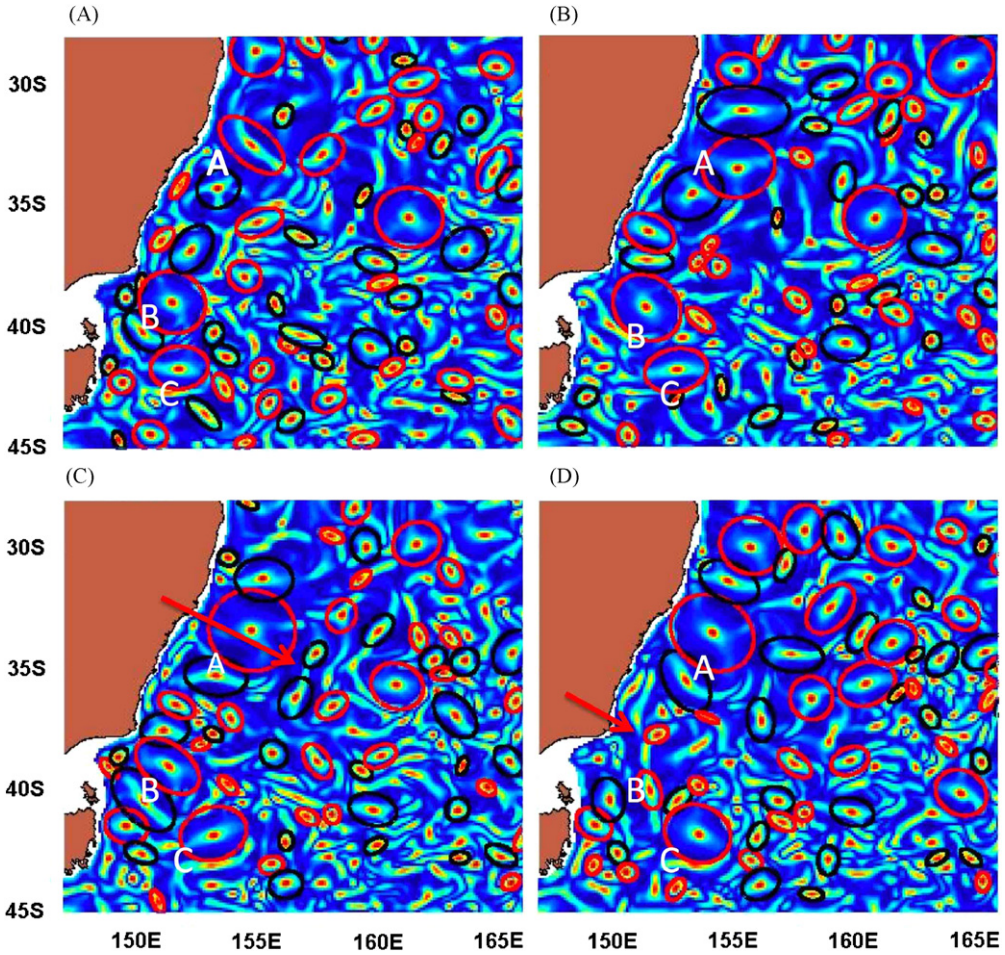

Fig. 10. Convolution of daily average surface velocities with a pattern template of symmetric rotation (Fig. 4A). The orientation and aspect ratio of large vortices is estimated with anticyclonic eddies (red) and cyclonic eddies (black). (A) 17 March, (B) 24 March, (C) 31 March and (D) 7 April. Labels A, B and C are used to track specific eddies. (For interpretation of the references to colour in this figure legend, the reader is referred to the web version of this article.)

at two-week intervals on 10 and 25 February, and 14 March 2008. During this experiment the EAC was observed by all six buoys which propagated south and traced the EAC separation from the coast (see Fig. 11). The two-week sampling of the buoys observed the transient reattachment of the EAC separation point.

The corresponding simulation of 24 h mean sea-level anomaly and surface currents from OceanMAPS (Brassington et al., 2007a) is shown in Figs. 12 and 13 for the period of the simulation at a time interval of 7 days. Overlayed on each image is the Lagrangian trajectories of all drifting buoys in the region within ± 2 days from the date of the image. The buoys are assigned different colours according to their origin: from the 2008 experiment (red), 2007 experiment (blue) and the global array (black).

The first buoy pair observed a separation point at a latitude of 31°S with a flow extension that recirculated north before continuing to propagate east (see Fig. 11). The buoy pair showed a small change in separation distance whilst within the EAC, indicating this flow is approximately non-dispersive. The trajectories for this buoy pair are shown in 5-day segments in Fig. 12A–D. Fig. 12A and B shows that a separation point is simulated by a front with a cyclonic eddy; however, the position of the separation point in the model lags the observed separation point. The recirculation of the buoys is represented in the simulations by a front with a surface depression and orbits the cyclonic circulation in Figs. 12B–D and 13A–C.

The second pair observed a similar separation point; however, the flow extension had unfolded to an easterly direction

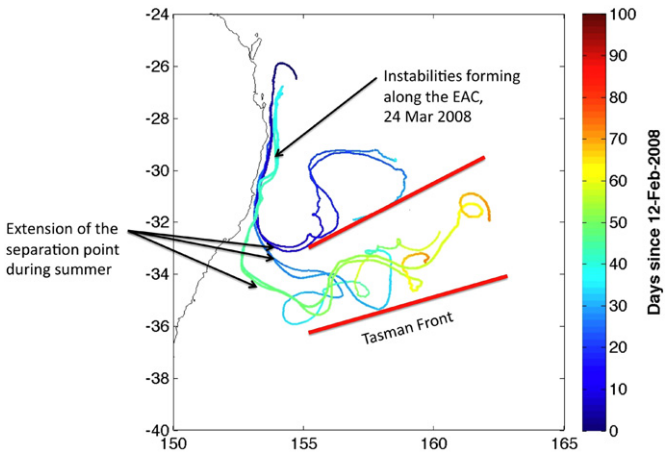

Fig. 11. Observed trajectories of six drifting buoys for the first 100 days since the first deployment on 10 February 2008. The buoys were deployed as pairs separated by ~5 km on 10 and 25 February and 14 March. The colour of the trajectories indicates the time of the observation since the initial deployment. (For interpretation of the references to colour in this figure legend, the reader is referred to the web version of this article.)

propagating along a classical Tasman front (see Fig. 11). In this instance the buoys observed a flow saddle point and a maximum flow dispersion at approximately 157°E,35°S. The buoys observe

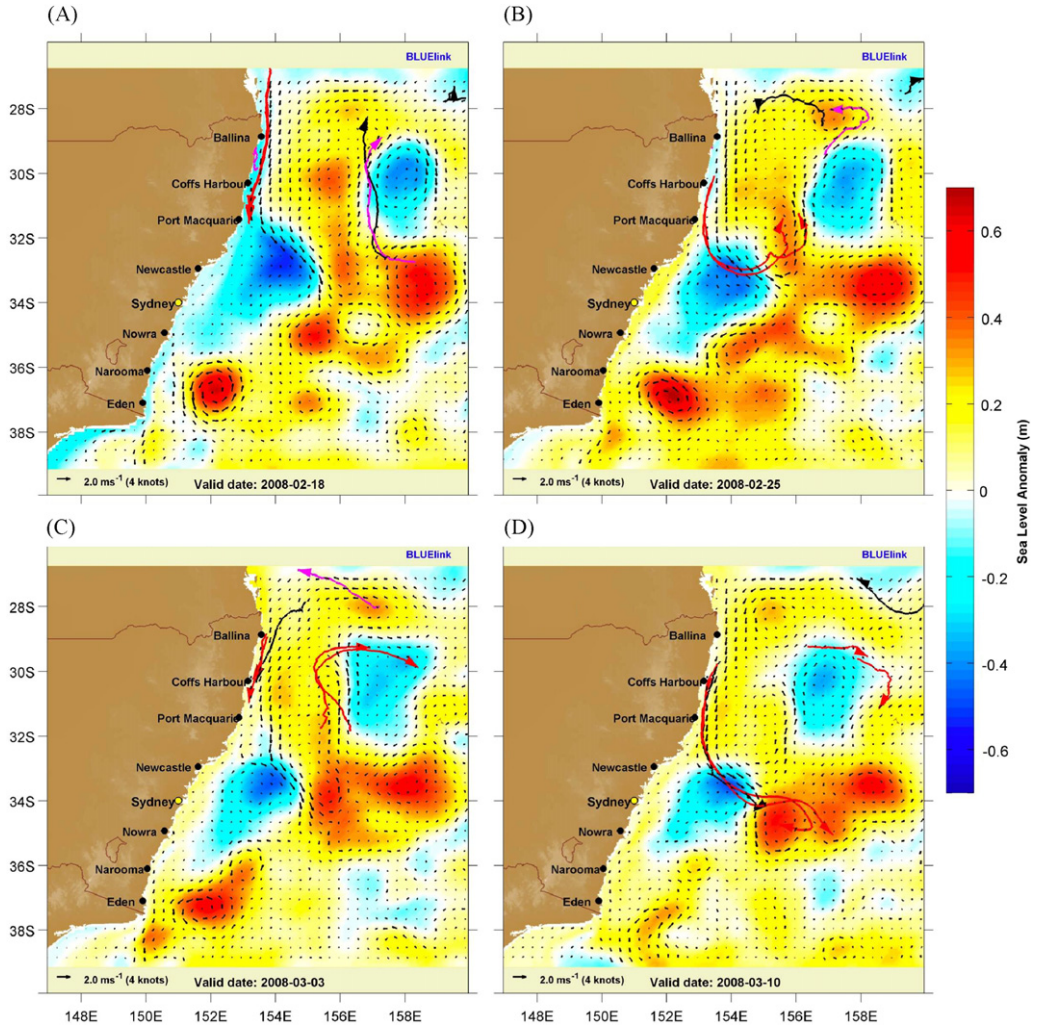

Fig. 12. Sea-level anomaly and surface currents from the BLUElink OceanMAPS analysis for (A) 18 February and (B) 25 February, and (C) 3 March and (d) 10 March 2008. Overlayed are the trajectories of drifting buoys for ± 2 days from the date of the image. Buoys are shown in (red) 2008 experiment, (magenta) 2007 experiment and (black) other buoys from the global array. (For interpretation of the references to colour in this figure legend, the reader is referred to the web version of this article.)

the circulation of smaller scale eddies, which are poorly represented in the OceanMAPS surface currents in Fig. 13A–C.

The third buoy pair observes a distinctly higher-latitude separation point of 33°S, which is within the range of latitudes identified by Godfrey et al. (1980). The separation is observed to be near perpendicular to the coastline, indicating a sharp front. The simulation however shows a weakened front and surface current in Fig. 13C. The flow extension continues eastward in a position along the Tasman front. The flow extension in this case was observed to be stable with low flow dispersion (i.e. small separation distance between the two buoys). The simulation from OceanMAPS (Brassington et al., 2007a) shows that the separation point and flow extension was related to a large cyclonic eddy off the NSW coast. The southern propagation of the separation point and flow extension corresponds to a southern displacement of the cyclonic vortex. During the reattachment the separation becomes more acute from the coastline, indicating that further southward propagation of the separation point is being limited by a cyclonic eddy. The timescale for this transient reattachment is on the order of 7 weeks.

An important feature of the third buoy pair is the observed perturbation to the EAC at the lower latitude of ~30°S. This disturbance is associated with a coastal cyclonic circulation and a cool sea surface temperature anomaly (not shown). This disturbance occurred at approximately the same position to that observed in 2007 and shown in Figs. 4, 5 and 7. The consistency of the position for these disturbances indicates that during this period, when the EAC is fully developed, it is sensitive to flow perturbations off the northern NSW coast leading to frequent flow instabilities.

4. Conclusion

A transient separation event of the EAC was observed to occur during March 2007. The event involved a warm-core anticyclonic eddy propagating within the EAC mean flow between 26 and 29°S where it encountered a cyclonic circulation anomaly over the continental shelf. The anticyclonic eddy surface circulation was observed by a pair of drifting buoys throughout the separation event. The cyclonic circulation was observed as a cool surface anomaly at ~29.5°S and was simulated by the BRANv2.2 as a local depression in sea level. Composited MTSAT SST observations show a narrow cool filament of SST that traces the outer edge of the cyclonic circulation and frontal boundary. The anticyclonic eddy and cyclonic eddy formed a dipole with a direction of propagation away from the coast. The MTSAT SST on 9 March continued to show the cool trace of the cyclonic circulation that

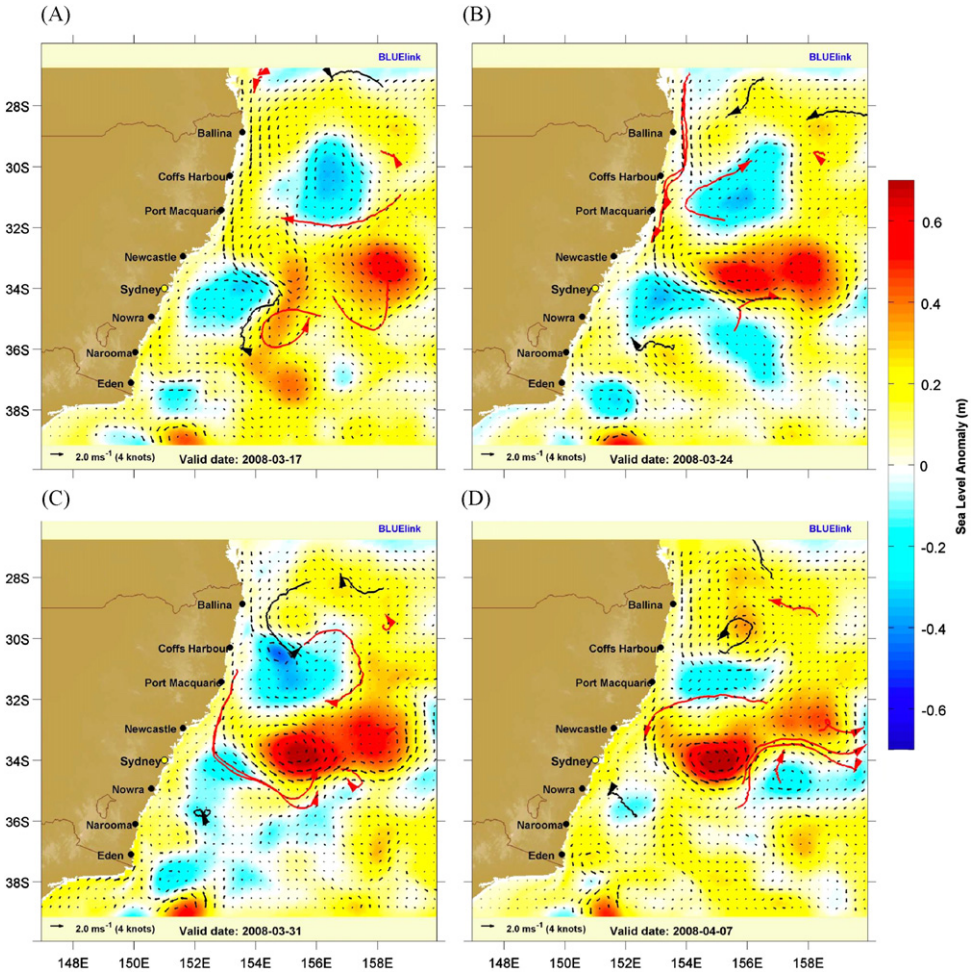

Fig. 13. Sea-level anomaly and surface currents from the BLUElink OceanMAPS analysis for (A) 17 March, (B) 24 March, (C) 31 March and (D) 7 April 2008. Overlayed are the trajectories of drifting buoys for ± 2 days from the date of the image. Buoys are shown in (red) 2008 experiment, (magenta) 2007 experiment and (black) other buoys from the global array. (For interpretation of the references to colour in this figure legend, the reader is referred to the web version of this article.)

propagates off the shelf with the anticyclonic eddy. The pair of drifting buoys remained within the surface circulation of the anticyclonic eddy throughout the separation from the coast and observed a maximum eddy propagation speed of 0.4 m s^{-1} (Brassington, 2010) on 16 March.

The formation of local cyclonic circulation between Ballina and Coffs Harbour along the Australian east coast was observed on 24 March 2008, the same month as the year earlier. Two drifting buoys deployed within the EAC on 14 March observed a transient perturbation in response to this cyclonic anomaly over the shelf (see Fig. 13B). Similarly, a cool anomaly in SST was also observed (Brassington et al., 2008; see Fig. 7). The formation of this feature occurred in less than two weeks, the time interval of an earlier buoy pair deployed in the EAC that exhibited no perturbation. A mechanism that forms cool anomalies over the shelf is coastal upwelling. Coastal upwelling occurs frequently along the east coast of Australia (e.g., Oke and Middleton, 2001). In the two cases above, upwelling favourable winds were observed over the continental shelf (not shown) for 3 days between 16 and 18 March 2007 preceding the 2007 event. Upwelling favourable winds were also observed for four days between 19 and 20 March 2008 preceding the 2008 event. Other mechanisms related to the EAC interaction with the shelf have also been identified (Roughan and Middleton, 2002). Once a perturbation has formed, the subsequent dynamic interaction with the EAC and the potential unstable growth requires further investigation for impacts to both local coastal shelf circulation and general circulation of the EAC.

The anticyclonic eddy separation event in 2007 propagated away from the coast to a position of rest at approximately 157.5°E,31.2°S. During this time the SST observations show an isolated warm anomaly (see Fig. 7H) consistent with the material ellipse estimated from the two drifting buoys. The BRAN2.2 analysis indicates a positive surface anomaly propagates to the resting position from the southwest ahead of the surface eddy (see Fig. 5A–D). Upon arrival of the separated eddy a vortex merger takes place resulting in a larger surface anomaly both in magnitude and horizontal extent. The drifting buoys behaviour prior and post merger support the hypothesis that the eddies underwent a stratified merger. Firstly, the two buoys remained within the surface circulation without a discontinuity to the material surface properties. Secondly, the material ellipse reduces in surface area subsequent to merger, indicating vertical motion and adjustment between the two eddies. The Argo repeat profiles also clearly show that subsequent to merger the vortex shows a T/S anomaly to a depth exceeding 500 m. This is deeper than the shelf slope which would constrain the depth of EAC eddy.

A stratified vortex merger in the Tasman Sea has been previously observed (Cresswell, 1982), indicating that such events may be prevalent in the Tasman Sea. A pattern matching method was applied to BRAN2.2 to visualise the 3-dimensional

extent of the eddies represented in the analysis (see Fig. 9). Any snapshot of the analysis will show a large number of vortices of both cyclonic and anticyclonic circulations. The surface layer shows the highest concentration of vortices of varying depth scale up to full depth. The pattern matching algorithm used here does not discriminate for rotational speed and as expected the speed declines with depth. Below the surface layer (<200 m) there remains a lower but significant concentration of vortices which includes full depth eddies and residual motion that have sheered from the surface eddy. There is only a couple of observational cases for sub-surface vortices in the Tasman Sea that undergo vortex mergers. This evidence is too limited to verify or reject the distribution of abyssal vortices and frequency of stratified vortex mergers represented in the ocean analysis. The deep ocean is constrained by a sparse network of profiles together with vertical projection of surface observations of sea surface height anomaly and SST. A high-resolution multi-instrument observational campaign for a region sufficient to include multiple eddies and a period sufficient to capture eddy–eddy interactions will be required to obtain definitive evidence. Such campaigns would include a fleet of ocean gliders (e.g., Baird et al., 2011), an array of bottom mounted ADCPs and inverted echo sounder (e.g., Donohue et al., 2010) and surface drifting buoys. Resolving the vertical structure of the Tasman Sea eddies and interactions has practical implications for ocean state estimation and circulation.

Drifting buoys provide high temporal sampling of the upper-layer circulation and in situ measurements of bulk SST that are complementary to other components of the observing system. The deployment of drifting buoys into the Tasman Sea declined in the 1990s. A renewed observing campaign was initiated in 2007 through a collaboration of the Bureau of Meteorology and the National Oceanographic and Atmospheric Administration to deploy surface drifting buoys to observe the East Australian Current and the Tasman Sea circulation. The residence time for drifting buoys within the EAC as expected is short, therefore a repeat deployment strategy was undertaken to increase the frequency of the EAC observations. An objective of the campaign was to identify a low-cost and robust method for deployment that could be sustained and also yield high-quality observations of the EAC and the Tasman Sea. Standard drifting buoys have been designed to be easy to deploy by volunteer observers permitting their deployment from the volunteer observing ship network. The PX30 XBT line was identified as being a suitable deployment location as it transects the EAC at a section of coast where it is statistically semi-permanent. The PX30 XBT line is occupied by two volunteer ship offering repeat deployments on a two-week frequency. The buoys deployed in the past three years have successfully observed dipole separation from the coast, stratified vortex merger, secondary circulation and surface divergence of an EAC anticyclonic eddy and the transient propagation of the separation point of the EAC. Future deployments in the Tasman Sea are likely to focus on addressing questions related to the impact of drifting buoys to state estimation and deployment strategies through intensive observation campaigns.

Acknowledgments

The authors thank the BLUElink science team, Bureau of Meteorology and CSIRO for use of the BLUElink model products. We gratefully acknowledge Lisa Cowen and Graeme Ball from the Bureau of Meteorology, Rick Lumpkin from the NOAA and the crew of both the Forum Samoa II and the Capitaine Tasman for assisting in the coordination of the drifting buoy experiments described. We gratefully acknowledge Dr. George Cresswell's communications on the history of drifting buoys and mesoscale studies in the Tasman Sea. We gratefully acknowledge Dr. Leon Majewski from the Bureau of Meteorology for processing of the MTSAT data products made available by JAXA. OSTIA data are published by the Met Office (http://www.metoffice.gov.uk) as a UK contribution to the GODAE High Resolution SST Pilot Project (GHRSST-PP, http://www.ghrsst-pp.org) and are © Crown Copyright 2007.

References

Airey, D., 1983. Isothermal temperatures and transformations of the warm-core eddies in the western Tasman Sea. Aust. J. Mar. Freshw. Res. 34, 681–685.

Andrews, J.C., Scully-Power, P., 1976. The structure of an East Australian Current anticyclonic eddy. J. Phys. Oceanogr. 6, 756–765.

Baird, M.E., Suthers, I.M., Griffin, D.A., Hollings, B., Pattiaratchi, C., Everett, J.D., Roughan, M., Oubelkheir, K., Doblin, M., 2011. The effect of surface flooding on the physical-biogeochemical dynamics of a warm core eddy off southeast Australia. Deep Sea. Res. II 58 (5), 592–605.

Bambrey, R.R., 2007, Strong interactions between two co-rotating vortices in rotating and stratified flows. Ph.D. Thesis, St Andrews.

Beron-Vera, F.J., Olascoaga, M.J., Brown, M.G., 2003. Passive tracer patchiness and particle trajectory stability in incompressible two-dimensional flows. Non-linear Proc. Geophys 1, 1–8.

Brassington, G.B., 2010. Estimating surface divergence of ocean eddies using observed trajectories from a surface drifting buoy. J. Atmos. Oceanic Technol. 27, 705–720, doi:10.1175/2009JTECHO651.1.

Brassington, G.B., Pugh, T., Spillman, C., Schulz, E., Beggs, H., Schiller, A., Oke, P.R., 2007a. BLUElink: development of operational oceanography and servicing in Australia. J, Res. Pract. Inform. Technol. 39, 151–164.

Brassington, G.B., Summons, N., Ball, G., Cowen, L., 2007b. East Australian Current and Tasman Sea pilot surface drifting buoy experiment. BMRC Res. Lett. 6, 21–25 〈http://www.bom.gov.au/bmrc/pubs/researchletter/reslett_06.pdf〉.

Brassington, G.B., Summons, N., Ball, G., Cowen, L., 2008. East Australian Current and Tasman Sea pilot surface drifting buoy experiment—2008. CAWCR Res. Lett. 1, 14–18 〈http://www.cawcr.gov.au/publications/researchletters/CAWCRResLets1.pdf〉.

Capet, X., McWilliams, J.C., Molemaker, M.J., Shchepetkin, A.F., 2008. Mesoscale to submesoscale transition in the California Current system. Part II: frontal processes. J. Phys. Oceanogr. 38, 44–64, doi:10.1175/2007JPO3671.1.

Chiswell, S.M., 2009. Colonisation and connectivity by intertidal limpets among New Zealand, Chatham and Sub-Antarctic Islands. II. Oceanographic connections. Mar. Ecol. Progr. Ser. 388, 121–135 doi:110.3354/meps08167.

Chiswell, S.M., Rickard, G.J., 2008. Eulerian and Lagrangian statistics in the Bluelink numerical model and AVISO altimetry: validation of model eddy kinetics. J. Geophys. Res. 113, C10024 doi:10010.11029/12007JC004673.

Church, J.A., 1987. East Australian Current adjacent to the Great Barrier Reef. Aust. J. Mar. Freshw. Res. 38, 671–683, doi:10.1071/MF9870671.

Cresswell, G., 1980. Physical evolution of Taman Sea eddy. Aust. J. Mar. Freshw. Res. 34 (4), 495–513, doi:10.1071/MF9830495.

Cresswell, G., 1982. The coalescence of two East Australian Current warm-core eddies. Science 215, 161–164.

Cresswell, G.R., Golding, T.J., 1979. Satellite-tracked buoy data report III. Indian Ocean 1977, Tasman Sea releases July–December 1977. CSIRO Aust. Div. Fish. Oceanogr., Rep. 101, p. 248.

Cresswell, G.R., Legeckis, R., 1986. Eddies off southeastern Australia. Deep-Sea Res. 33, 1527–1562, doi:10.1016/0198-0149(86)90066-X.

Davidson, F., Allen, A., Brassington, G.B., Breivik, O., Daniel, P., Kamachi, M., Sato, S., King, B., Lefevre, F., Sutton, M., Kaneko, H., 2009. Application of GODAE ocean current forecasts to search and rescue and ship routing. Oceanography 22 (3), 176–181.

Donlon, C.J., Minnet, P.J., Gentemann, C., Nightingale, T.J., Barton, I.J., Ward, B., Murray, M.J., 2002. Toward improved validation of satellite sea surface skin temperature measurements for climate research. J. Climate 15, 353–369.

Donlon, C.J., Casey, K.S., Robinson, I.S., Gentemann, C.L., Reynolds, R.W., Barton, I.J., Arino, O., Stark, J., Rayner, N., LeBorgne, P., Poulter, D., Vazquez-Cuervo, J., Armstrong, E., Beggs, H., Llewellyn-Jones, D., Minnett, P.J., Merchant, C.J., Evan, R., 2009. The GODAE high-resolution sea surface temperature pilot project. Oceanography 22 (3), 34–45.

Donohue, K.A., Watts, D.R., Tracey, K.L., Greene, A.D., Kennelly, M., 2010. Mapping circulation in the Kuroshio extension with an array of current and pressure recording inverted echo sounders. J. Atmos. Oceanic Technol 27, 507–527, doi:10.1175/2009JTECHO686.1.

Ducet, N., Le Traon, P.-Y., Reverdin, G., 2000. Global high-resolution mapping of ocean circulation from TOPEX/Poseidon and ERS1 and -2,. J. Geophys Res. 105 (C8), 19477–19498, doi:10.1029/2000JC900063.

Ebling, J., Scheuermann, G., 2003, Clifford convolution and pattern matching on vector fields. In: the Proceedings of IEEE Visualization'03, Los Alamos, CA. IEEE Computer Society, doi:10.1109/VISUAL.2003.1250372.

Ebling, J., Scheuermann, G., 2005. Clifford fourier transform on vector fields. IEEE Trans. Vis. Comput. Graph. 11 (4), 469–479, doi:10.1109/TVCG.2005.54.

Font, J., Isern-Fontanet, J., de Jesus Salas, J., 2004. Tracking a big anticyclonic eddy in the western Mediterranean Sea. Sci. Mar. 68, 331–342, doi:10.3989/scimar.2004.68n3331.

Fu, L.-L., Alsdorf, D., Rodriguez, E., Morrow, R., Mognard, N., Lambin, J., Vaze, P., Lafon, T., 2009. The SWOT (Surface Water and Ocean Topography) Mission: spaceborne radar interferometry for oceanographic and hydrological applications. In: OCEANOBS'09 Conference.

Godfrey, J.S., 1989. A Sverdrup model of the depth-integrated flow for the world ocean allowing for island circulations. Geophys. Astrophys. Fluid Dynam. 45, 89–112.

Godfrey, J.S., Cresswell, G.R., Golding, T.J., Pearce, A.F., Boyd, R., 1980. Separation of the East Australian Current. J. Phys. Oceanogr. 10, 430–440.

Griffies, S.M., Harrison, M.J., Pacanowski, R.C., Rosati A., 2003. A technical guide to mom4 gfdl ocean group technical report no. 5, NOAA/Geophysical Fluid Dynamics Laboratory Version prepared on December 23, 2003.

Hackett, B., Comerma, E., Daniel, P., Ichikawa, H., 2009. Marine oil pollution prediction. Oceanography 22 (3), 160–175.

Heiberg, E.B., 2001, Automated feature detection in multidimensional images. Linkoping Studies in Science and Technology, Thesis No. 909. Department of Biomedical Engineering & Medicine and Care, Linkoping University, Sweden.

Hernandez, F., Le Traon, P.-Y., Morrow, R., 1995. Mapping mesoscale variability of the Azores current using TOPEX/Poseidon and ERS-1 altimetry, together with hydrographic and Lagrangian measurements. J. Geophys Res. 100, 24995–25006, doi:10.1029/95JC02333.

Laing, A.K., Challenor, P.G., 1999. Estimation of the mean dynamic height from altimeter profiles and hydrography. J. Atmos. Oceanic Technol. 16, 1873–1879 doi:10.1175/1520-0426.

Lumpkin, R., Pazos, M., 2007. In: Griffa, A., Kirwan, D., Mariano, A., Ozgokmen, T., Rossby., T. (Eds.), Measuring surface currents with surface velocity program drifters: the instrument, its data and some recent results. Cambridge University Press, pp. 2007.

Marchesiello, P., Middleton, J.H., 2000. Modelling the East Australian Current in the western Tasman Sea. J. Phys. Oceanogr. 30, 2956–2971.

McInnes, K.M., Leslie, L.M., McBride, J.L., 1992. Numerical simulation of cut-off lows on the Australian east coast: sensitivity to sea surface temperature. Int. J. Climatol. 12, 1–13, doi:10.1002/joc.3370120803.

Molcard, A., Ozokmen, T.M., Griffa, A., Piterbarg, L.I., Chin, T.M., 2007. In: Griffa, A., Kirwan, D., Mariano, A., Ozgokmen, T., Rossby., T. (Eds.), Lagrangian data assimilation in ocean general circulation models. Cambridge University Press.

Niiler, P., 2001. Global ocean circulation observations. In: Koblinsky, C.J., Smith, N.R. (Eds.), Observing the Oceans in the 21st century. GODAE Project Office, Bureau of Meteorology, pp. 307–323.

Niiler, P.P., Sybrandy, A., Bi, K., Poulain, P., Bitterman, D., 1995. Measurements of the water-following capability of Holey-sock and TRISTAR drifters. Deep-Sea Res. 42, 1951–1964, doi:10.1016/0967-0637(95)00076-3.

Nilsson, C.S., Andrews, J.C., Scully-Power, P., 1977. Observations of eddy formation off East Australia. J. Phys. Oceanogr. 7, 659–669.

Nilsson, C.S., Cresswell, G.R., 1981. The formation and evolution of East Australian Current warm-core eddies. Prog. Oceanogr. 9, 133–183, doi: 10.1016/0079-6611(80)90008-7.

Oke, P.R., Balmaseda, M.A., Benkiran, M., Cummings, J.A., Dombrowsky, E., Fujii, Y., Guinehut, S., Larnicol, G., Le Traon, P.-Y., Martin, M., 2009. Observing system evaluations using GODAE systems. In: The revolution in global ocean forecasting—GODAE: 10 years of achievement. Oceanography 22, 144–153.

Oke, P.R., Brassington, G.B., Griffin, D.A., Schiller, A., 2008. The Bluelink ocean data assimilation system (BODAS). Ocean Model. 21, 46–70, doi:10.1016/j.ocemod.2007.11.002.

Oke, P.R., Middleton, J.H., 2001. Nutrient enrichment off Port Stephens: the role of the East Australian Current. Cont. Shelf Res. 21, 587–606, doi: 10.1016/S0278-4343(00)00127-8.

Oke, P.R., Middleton, J.H., 2000. Topographically induced upwelling off Eastern Australia. J. Phys. Oceanogr. 30, 512–531.

Okubo, A., 1970. Horizontal dispersion of floatable particles in the vicinity of velocity singularities such as convergences. Deep-Sea Res 17, 445–454, doi:10.1016/0011-7471(70)90059-8.

Pasquero, C., Bracco, A., Provenzale, A., Weiss, J.B., 2007. Particle motion in a sea of eddies. In: Griffa, A., Kirwan, D., Mariano, A., Ozgokmen, T., Rossby., T. (Eds.), Lagrangian Analysis and Prediction of Coastal and Ocean Dynamics. Cambridge University Press.

Provenzale, A., 1999. Transport by coherent barotropic vortices. Annu. Rev. Fluid Mech. 31, 55–93.

Reinaud, J.N., Dritschel, D.G., 2002. The merger of vertically offset quai-geostrophic vortices. J. Fluid Mech. 469, 287–315, doi:10.1017/S0022112002001854.

Richardson, P.L., Bower, A.S., Zink, W., 2000. A census of M eddies tracked by floats. Prog. Oceanogr 45, 209–250, doi:10.1016/S0079-6611(99)00053-1.

Ridgway, K.R., Dunn, J.R., 2003. Mesoscale structure of the mean East Australian Current system and its relationship to topography. Prog. Oceanogr 36, 189–222, doi:10.1016/S0079-6611(99)00053-1.

Ridgway, K.R., Godfrey, J.S., 1997. Seasonal cycle of the East Australian Current. J. Geophys. Res. 102 (C10), 22921–22936, doi:10.1029/97JC00227.

Roughan, M., Middleton, J.H., 2002. A comparison of observed upwelling mechanisms off the east coast of Australia. Cont. Shelf Res. 22 (17), 2551–2572, doi:10.1016/S0278-4343(02)00101-2.

Rupolo, V., 2007. In: Griffa, A., Kirwan, D., Mariano, A., Ozgokmen, T., Rossby., T. (Eds.), Observing turbulence regimes in the oceans. Cambridge University Press.

Sangra, P., Pelegri, J.L., Hernandez-Guerra, A., Arregui, I., Martin, J.M., Marrero-Diaz, A., Martinez, A., Ratsimandresey, A.W., Rodriguez-Santana, A., 2005. Life history of an anticyclonic eddy. J. Geophys. Res. 110, 3021–3039, doi:10.1029/2004JC002526.

Schiller, A., Oke, P.R., Brassington, G.B., Entel, M., Fiedler, R.A.S., Griffin, D.A., Mansbridge, J.V., Meyers, G.A., Ridgway, K.R., Smith, N.R., 2008. Eddy-resolving ocean circulation in the Asia–Australian region inferred from an ocean reanalysis effort. Prog. Oceanogr 76, 334–365, doi:10.1016/j.pocean.2008.01.003.

Seaman, R., Bourke, W., Steinle, P., Hart, T., Embery, G., Naughton, M., Rikus, L., 1995. Evolution of the Bureau of Meteorology's global assimilation and prediction system, Part 1: analyses and initialization. Aust. Met. Mag 44, 1–18.

Stammer, D., 1997. Global characteristics of ocean variability from regional TOPEX/POSEIDON altimeter measurements. J. Phys. Oceanogr 27, 1743–1769.

Stark, J.D., Donlon, C.J., Martin M.J., McCulloch M.E., 2007, OSTIA: an operational, high resolution, real time, global sea surface temperature analysis system. In: Oceans'07 IEEE Aberdeen, Conference Proceedings. Marine Challenges: Coastline to Deep Sea, Aberdeen, Scotland. IEEE, doi:10.1109/OCEANSE.2007.4302251.

Summons, N., Brassington, G.B., Simmonds, I., 2006. A survey of the surface drifter observation record for Australia's current systems. BMRC Res. Lett. 5, 12–17 〈http://www.bom.gov.au/bmrc/pubs/researchletter/reslett_05.pdf〉.

Tilburg, C.E., Hurlburt, H.E., O'Brien, J.J., Shriver, J.F., 2001. The dynamics of the East Australian Current system: the Tasman Front, the East Auckland Current, and the East Cape Current. J. Phys. Oceanogr. 31, 2917–2943.

Tranter, D.J., Carpenter, D.J., Leech, G.S., 1986. The coastal enrichment effects of the East Australian Current eddy field. Deep Sea Res. 33, 1705–1728, doi:10.1016/0198-0149(86)90075-0.

Weiss, J.B., 1991. The dynamics of enstrophy transfer in two-dimensional hydrodynamics. Physica D 48, 273–294, doi:10.1016/0167-2789(91)90088-Q.

Wilkin, J.L., Zhang, W.G., 2007. Modes of mesoscale sea surface height and temperature variability in the East Australian Current. J. Geophys. Res. 112, C01013. doi:10.1029/2006JC003590.